# REPORT DOCUMENTATION PAGE

Form Approved OMB NO. 0704-0188



| 1. REPORT DATE (DD-MM-YYYY) | 2. REPORT TYPE | 3. DATES COVERED (From - To) |
|---|---|---|
| 15-05-2017 | Final Report | 1-Aug-2013 - 31-Jul-2016 |

4. TITLE AND SUBTITLE

FINAL Report: Nanoelectromechanical Oscillator Arrays: A Laboratory for Synchronization on Lattices and Networks

5a. CONTRACT NUMBER
W911NF-13-1-0240

5b. GRANT NUMBER

5c. PROGRAM ELEMENT NUMBER
611102

6. AUTHORS

Michael Roukes, Michael Cross, Matthew Matheny, Warren Fon

5d. PROJECT NUMBER

5e. TASK NUMBER

5f. WORK UNIT NUMBER

7. PERFORMING ORGANIZATION NAMES AND ADDRESSES

California Institute of Technology
Office of Sponsored Research
1200 E. California Blvd.
Pasadena, CA 91125 -0001

8. PERFORMING ORGANIZATION REPORT NUMBER

9. SPONSORING/MONITORING AGENCY NAME(S) AND ADDRESS (ES)

U.S. Army Research Office
P.O. Box 12211
Research Triangle Park, NC 27709-2211

10. SPONSOR/MONITOR'S ACRONYM(S)
ARO

11. SPONSOR/MONITOR'S REPORT NUMBER(S)
63679-EG.1

12. DISTRIBUTION AVAILIBILITY STATEMENT

Approved for Public Release; Distribution Unlimited

13. SUPPLEMENTARY NOTES

The views, opinions and/or findings contained in this report are those of the author(s) and should not contrued as an official Department of the Army position, policy or decision, unless so designated by other documentation.

14. ABSTRACT

Control of the global parameters of complex networks has been explored experimentally in a variety of contexts. Yet, the more difficult prospect of realizing arbitrary network architectures, especially analog physical networks, that provide dynamical control of individual nodes and edges has remained elusive. It also proves challenging to measure a complex network's full internal dynamics given the vast hierarchy of timescales involved. These span from the fastest nodal dynamics to very slow epochs over which emergent global phenomena, including network synchronization and the manifestation of exotic steady states, eventually emerge. In this effort we have realized and

15. SUBJECT TERMS

NEMS, Synchronization, Networks, Control

| 16. SECURITY CLASSIFICATION OF: | | | 17. LIMITATION OF ABSTRACT | 15. NUMBER OF PAGES | 19a. NAME OF RESPONSIBLE PERSON |
|---|---|---|---|---|---|
| a. REPORT | b. ABSTRACT | c. THIS PAGE | | | Michael Roukes |
| UU | UU | UU | UU | | 19b. TELEPHONE NUMBER 626-395-2916 |

## Report Title

FINAL Report: Nanoelectromechanical Oscillator Arrays: A Laboratory for Synchronization on Lattices and Networks


## ABSTRACT

Control of the global parameters of complex networks has been explored experimentally in a variety of contexts. Yet, the more difficult prospect of realizing arbitrary network architectures, especially analog physical networks, that provide dynamical control of individual nodes and edges has remained elusive. It also proves challenging to measure a complex network's full internal dynamics given the vast hierarchy of timescales involved. These span from the fastest nodal dynamics to very slow epochs over which emergent global phenomena, including network synchronization and the manifestation of exotic steady states, eventually emerge. In this effort we have realized and demonstrated an experimental system satisfying these requirements. It is based upon modular, fully controllable, nonlinear radio-frequency nanomechanical oscillators, designed to form the nodes of complex dynamical networks with edges configured with arbitrary topology. The dynamics of these oscillators and their surrounding network are analog, continuous-valued and can be fully interrogated in real time. Our embodiment permits network interconnections solely in the electrical domain, and provides unprecedented node and edge control over a vast region in parameter space. Continuous measurement of the instantaneous amplitudes and phases of every constituent oscillator node are enabled, yielding full and detailed network data without reliance upon statistical quantities.


---

## Enter List of papers submitted or published that acknowledge ARO support from the start of the project to the date of this printing. List the papers, including journal references, in the following categories:

### (a) Papers published in peer-reviewed journals (N/A for none)

| Received | Paper |
|---|---|

**TOTAL:**

**Number of Papers published in peer-reviewed journals:**

---

### (b) Papers published in non-peer-reviewed journals (N/A for none)

| Received | Paper |
|---|---|

**TOTAL:**

**Number of Papers published in non peer-reviewed journals:**

## (c) Presentations

Conference proceedings at two conferences.

1) SIAM CONFERENCE ON APPLICATIONS OF DYNAMICAL SYSTEMS 2015

Title: Synchronization of Nanomechanical Oscillators

Abstract:Synchronization, the mutual entrainment of limit cycle oscillators, is a ubiquitous phenomenon both in the physical and biological sciences. There exist many observation studies of this phenomenon; however, controlled experiments in this field are scant. In this talk, I will describe an experiment in synchronization based on NanoElectroMechanical (NEMS) oscillators. In addition to the ability to measure the amplitude and phase dynamics of individual nodes, the experiment demonstrates a large degree of control over the parameters of the system. Both the coherent and stochastic dynamics will be discussed.

2) 14th International Workshop on Nanomechanical Sensors 2017

Title: Synchronization of Nanomechancial Oscillators via Electronic Coupling

Abstract:Harnessing large networks of coupled nonlinear oscillators for sensing requires a deep understanding of the underlying network dynamics. Here, we will present a model system where network parameters can be tuned on a ‘microscopic’ level: synchronized arrays of self-sustaining, weakly anharmonic, nanomechanical oscillators. In our system, each oscillator is formed from a piezoelectric nanoplate individually mounted on printed circuit boards. In this paradigm, we show complete control over oscillator parameters while allowing for hot-plugging into networks. We will present experimental data involving oscillators coupled in ‘rings’, i.e. 1-D arrays with linear nearest-neighbor coupling and periodic boundary conditions.

**Number of Presentations:** 2.00

## Non Peer-Reviewed Conference Proceeding publications (other than abstracts):

| Received | Paper |
|---|---|

**TOTAL:**

**Number of Non Peer-Reviewed Conference Proceeding publications (other than abstracts):**

## Peer-Reviewed Conference Proceeding publications (other than abstracts):

| Received | Paper |
|---|---|

**TOTAL:**

**Number of Peer-Reviewed Conference Proceeding publications (other than abstracts):**

---

## (d) Manuscripts

Received Paper

**TOTAL:**

**Number of Manuscripts:**

---

## Books

Received Book

**TOTAL:**

Received Book Chapter

**TOTAL:**

## Patents Submitted

---

## Patents Awarded

---

## Awards

---

## Graduate Students

| NAME | PERCENT_SUPPORTED | DISCIPLINE |
|---|---|---|
| Raj Michael Katti | 14 | Physics |
| **FTE Equivalent:** | **0.14** | |
| **Total Number:** | **1** | |

## Names of Post Doctorates

| NAME | PERCENT_SUPPORTED |
|---|---|
| **FTE Equivalent:** | |
| **Total Number:** | |

## Names of Faculty Supported

| NAME | PERCENT_SUPPORTED | National Academy Member |
|---|---|---|
| Michael Roukes | 0.01 | |
| Michael Cross | 0.01 | |
| **FTE Equivalent:** | **0.02** | |
| **Total Number:** | **2** | |

## Names of Under Graduate students supported

| NAME | PERCENT_SUPPORTED | DISCIPLINE |
|---|---|---|
| Lev Krayzman | 50 | Physics, Computer Science |
| **FTE Equivalent:** | **0.50** | |
| **Total Number:** | **1** | |

## Student Metrics

This section only applies to graduating undergraduates supported by this agreement in this reporting period

The number of undergraduates funded by this agreement who graduated during this period: ..... 1.00

The number of undergraduates funded by this agreement who graduated during this period with a degree in science, mathematics, engineering, or technology fields:..... 1.00

The number of undergraduates funded by your agreement who graduated during this period and will continue to pursue a graduate or Ph.D. degree in science, mathematics, engineering, or technology fields:..... 1.00

Number of graduating undergraduates who achieved a 3.5 GPA to 4.0 (4.0 max scale):..... 0.00

Number of graduating undergraduates funded by a DoD funded Center of Excellence grant for Education, Research and Engineering:..... 0.00

The number of undergraduates funded by your agreement who graduated during this period and intend to work for the Department of Defense ..... 0.00

The number of undergraduates funded by your agreement who graduated during this period and will receive scholarships or fellowships for further studies in science, mathematics, engineering or technology fields: ..... 0.00

## Names of Personnel receiving masters degrees

| NAME |
|---|
| **Total Number:** |

## Names of personnel receiving PHDs

| NAME |
| --- |
| **Total Number:** |

## Names of other research staff

| NAME | PERCENT_SUPPORTED |
| --- | --- |
| Chung Wah (Warren) Fon | 0.25 |
| Edward Myers | 0.20 |
| Matthew Matheny | 0.12 |
| **FTE Equivalent:** | **0.57** |
| **Total Number:** | **3** |

## Sub Contractors (DD882)

## Inventions (DD882)

## Scientific Progress

See Attachment

## Technology Transfer

FINAL REPORT / ARO CONTRACT NO. **W911NF1310240**

# *NANOELECTROMECHANICAL OSCILLATOR ARRAYS*

## *A LABORATORY FOR SYNCHRONIZATION ON LATTICES AND NETWORKS*

MATT MATHENY, WARREN FON, MICHAEL CROSS, MICHAEL ROUKES (PI) – *CALTECH*

## INTRODUCTION

State-dependent networks, where states of both the system and the environment play critical roles, are of significant contemporary interest. Accordingly, it is important to develop experimental platforms for these efforts that can be upscaled to comprise a sufficiently large number of degrees-of-freedom that collective phenomena and emergent system properties become fully manifested. Further, as real-world systems are always subject both to internal fluctuations and to noisy and dynamic environments, a meaningful experimental platform must also incorporate such aspects. Finally, it is also essential to be able to investigate the evolution of network dynamics under deterministic perturbations, complex signal injection, and elemental nodal and edge control. Rich topologies involving layered networks, networks of networks, and adaptive network topologies (a new domain for network science) offer especially fertile ground for future explorations.

As a network's size increases and the topology of its connectivity becomes complex, its temporal evolution tends to span an increasingly vast hierarchy of time scales; these dynamics can often evolve over many decades in time. This poses a significant experimental challenge: to elucidate the richness of manifested phenomena one must track the *complete details* of the time evolution of the network – from its fastest "elemental" dynamics at every node, to the anomalous local-to-global diffusion of coherent and emergent synchronization patterns that are formed. For systems with many degrees-of-freedom, it is notoriously difficult to capture glassy dynamics; these generally evolve especially slowly, while remaining completely dependent on the fastest, nodal dynamics for their emergence. Further, the most interesting and important classes of emergent behaviors induced by system heterogeneity are generally impossible to predict *a priori*. For all of these domains, *experimental* investigations – guided and then analyzed within theoretical frameworks – are essential.

This project has been directed toward exploration of synchronization dynamics within an auspicious new platform: *coupled arrays of nanoelectromechanical systems (NEMS) oscillators*. NEMS networks provide the capability for reliably capturing the full complexity of nonlinear dynamics down to the detailed dynamics at individual constituent nodes, while permitting imposition of detailed perturbations from local to global scales. Since achieving complete observability of a NEMS network's complex internal dynamics is possible – including spanning the aforementioned hierarchy of time scales – it becomes possible to search for overarching system observables, that is, for *order parameters*, which best characterize emergent phenomena these complex systems manifest. Further, NEMS are truly analog and continuous-time, real-world systems. Modeling and capturing the true behavior of real-world systems often proves elusive (if not impossible!) by pursuits employing discrete numerical modeling or *digital* electronic systems. This is true because the dynamics of complex nonlinear systems are exquisitely (and notoriously) sensitive to minute perturbations. NEMS oscillators can be constructed to offer the benefit of having strong, precisely controllable

nonlinearities with easily tuned oscillation frequencies. These parameters are fundamental and essential to the dynamics of synchronization.

In the present work, we have achieved a significant and unprecedented milestone in the realization of complex networks of nonlinear NEMS oscillators. In this work, our oscillator "nodes" are each realized as a small, credit card sized printed circuit board (PCB) modules on which the frequency-determining element, a vacuum-encapsulated nonlinear NEMS resonator, is embedded within integrated circuit (IC) components for feedback and control. The modular PCBs offer the benefit of exquisite (high resolution) control and inexpensive amplification.

With our modular architecture, the NEMS oscillator modules are plugged into a larger "network" PCB that hosts the connections between oscillators – that is, the network's "edges". This enables continuous observation of each oscillator in the network as we modify, via electronic control, their parameters and their arbitrarily configured interconnections. Complete time records of the detailed phase evolution of every node can be acquired as the network transitions between unlocked, partially locked, and completely phase-locked states. Further, detailed dynamics -- including phase noise, phase slips, splay states, chimera states, *etc.* – can be directly and readily observed.

This "discrete" NEMS network platform we have achieved in this work serves as a prototype for future instantiations we envision, based on the co-integration of CMOS electronics with NEMS elements. Such future integrated architectures will easily transcend the limitations of our present discrete realization, which permits practical realization of up to ~100 nodes; massively upscaled networks, ultimately comprising tens of thousands of oscillator nodes, will become feasible.

# EXPERIMENTAL SYSTEM ACHIEVEMENTS

## SYSTEM OVERVIEW

The system design is shown in Figure 1. The experimental infrastructure has been developed from "scratch", specifically for this project. The cost is very low; roughly $200 per oscillator board (excluding fabrication of the NEMS resonator itself.)

The system can be approximately separated into the three functional layers illustrated in Figure 1. These are: a software/control layer, for operating the system; a digital-to-analog interface layer, comprised of both digital-to-analog outputs (for system control) and analog-to-digital inputs (to convert the nodal oscillator signals to digital data for readout); and an analog layer, comprising PCB-based coupling circuitry (the network edges) and PCB oscillator modules (the network nodes).

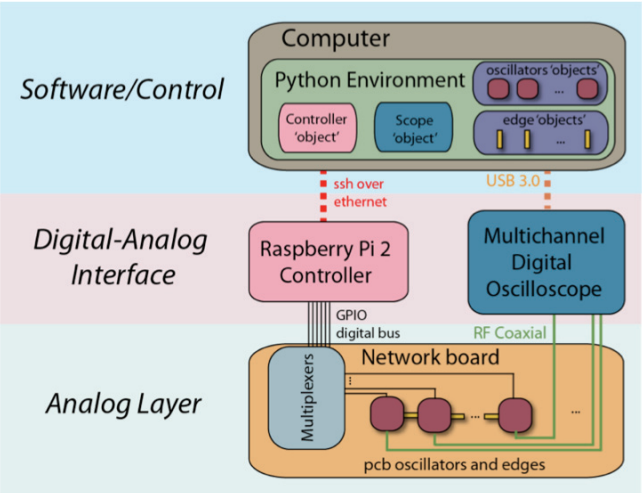


**Figure 1: System overview.** The system is comprised of three functional layers. The software/controller layer, the digital-analog interface, and the analog layer.

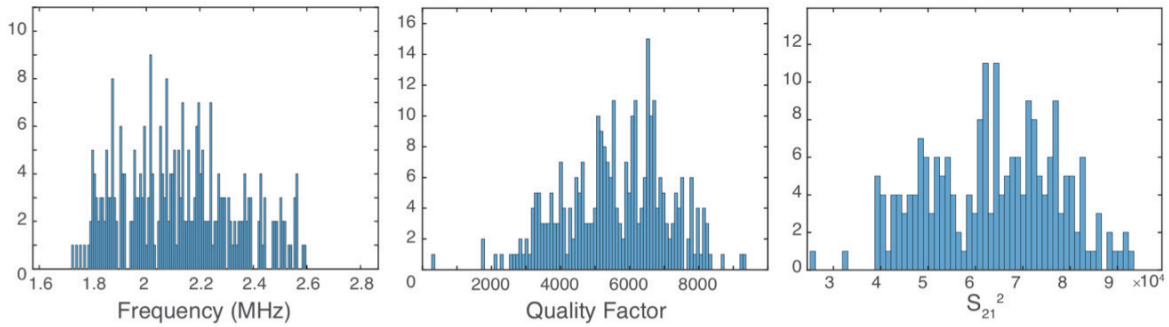


**Figure 2:** 'Linear' parameters of over 300 NEMS resonators, including measured frequencies, quality factors, and forward, *i.e.* input-to-output, scattering parameters (including amplification). Note that quality factor and forward scattering parameter, $S_{21}$, are highly correlated.

## ANALOG LAYER

Perfecting the analog side of the system proved to be the most challenging and novel part of the project. The analog layer is comprised of the oscillator modules and the network board into which they plug. Please see the report "*ARO Progress Report 2015*" [1] for complete information on our Generation-3 oscillator modules (which includes specifications for the NEMS resonators).

### *NEMS RESONATOR*

In the final year of this project, we shifted the NEMS resonator frequency from 7MHz down to 2MHz. Lowering this frequency facilitates incorporation of digital potentiometers (which have only modest working bandwidths) for nodal controls. We find this does not affect the dynamics, except that the ringdown time of the resonator shifts to 2ms given the lower resonance frequency. This changes the natural timescale of the network dynamics and also scales the coupling parameters by roughly a factor of 2.

We fabricated over 1000 devices for this project and fully tested more than 300 of the best of this "crop" for use in small networks. These tests were carried out to choose devices with parameters matched closely enough to readily permit coupling them using the external circuitry of the oscillator board. The results we achieved are shown in Figure 2. We selected first for quality factor, since this parameter is the most difficult to control in our current circuit design. These statistics presented are extremely important for understanding the number of devices that must be made in subsequent fabrication runs.

### *OSCILLATOR BOARD*

Figure 3a displays a block diagram of a single oscillator, showing its various components. The colors used in the two panels permit the components from the block diagram ("a") to be identified in the photograph of a PCB oscillator module ("b"). In our latest generation of oscillator board modules, we have removed all test points to reduce the effect of stray capacitance and improve performance.

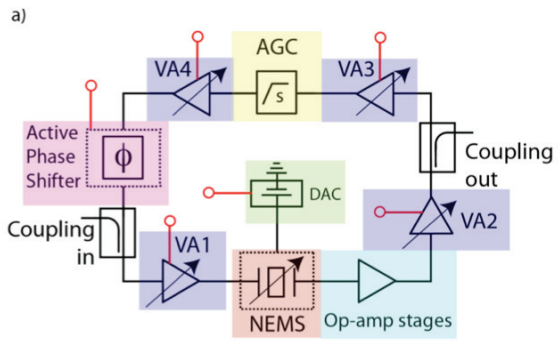


**Figure 3: A modular NEMS oscillator node.** a) Oscillator board diagram. b) Physical realization of oscillator board (5th gen). The colors in the diagram of a correspond to the color boxes surrounding the components in b).

Every adjustable component on the oscillator board can separately be digitally stepped to both increase conformity between oscillator modules and remove drift in controlling components. These controllable elements include: the digital step attenuators controlling signal levels, digital potentiometers to control phase shift in the loop, and digital-analog converters (DAC) to shift the frequency of the NEMS oscillators.

The red lines in Figure 3a indicate the location of digital control ports. In the previous year, we have changed the digital bus from I²C (inter-integrated circuit) to SPI (serial peripheral interface) protocol. This was done for several reasons. First, the digital step attenuators and DAC are formatted for operation under SPI, so an I²C-SPI bridge was previously necessary to communicate with these components. Second, most I²C components operate with bandwidth <1Mbit/s, limiting the speed at which we could shift nodal or network parameters. Finally, it is based on an open-drain design, which complicates multiplexing between many oscillators.

## OS CILLATOR BOARD BENCHMARKING

Our system relies on the strong agreement between our oscillator model (Matheny *et al.*, 2014) [2] and the measured performance of a single physical oscillator. A good indication of the agreement is obtained by ensuring that the oscillator amplitude v. frequency characteristic follows the Duffing model as the loop phase shift is swept. We show such a sweep in Figure 4. This demonstrates our ability to reliably control oscillator phase shift and oscillator amplitude.

Our network modeling is greatly simplified by first, *fabricating*, then subsequently, *tuning* the oscillators to be as similar as possible; this reduces network heterogeneity. In the absence of oscillator noise and coupling, the oscillators can be characterized by a quadratic "backbone" function (the quadratic and constant coefficient) delineated by the maxima of

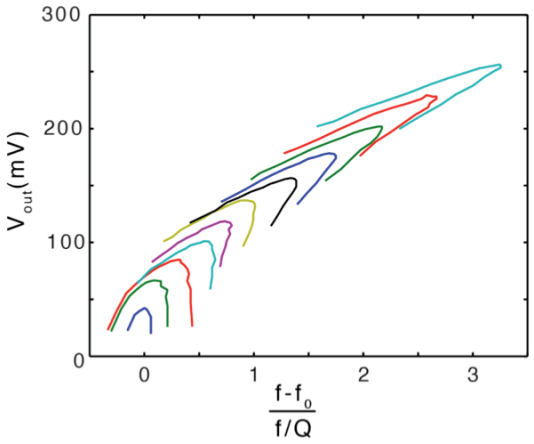


**Figure 4: Nonlinear NEMS oscillator performance.** The family of curves display changes in oscillator state for stepped AGC output (VA4 from figure 3,a). Normalized oscillator frequency deviation (x-axis) is controlled by sweeping loop phase shift; concomitantly, oscillator amplitude is maintained at maximal value. The family of curves here represents stepping the nonlinearity parameter $\alpha$ from approximately $.05 \rightarrow 3$.

the family of curves displayed in Figure 4. Figure 5 shows such backbone curves as output voltage (via VA2 in Fig. 3a) and DAC voltage (applied to the piezoelectric stack on the mechanical resonator, via VA1) are shifted. Thus, both the linear and nonlinear stiffness can be adjusted by controlling circuit parameters. In Figure 5, we show nonlinearity parameters ranging from $\alpha = .1 \rightarrow 6$. We discuss below (results section) why this range of nonlinearity is appropriate for the synchronization dynamics of interest to us.

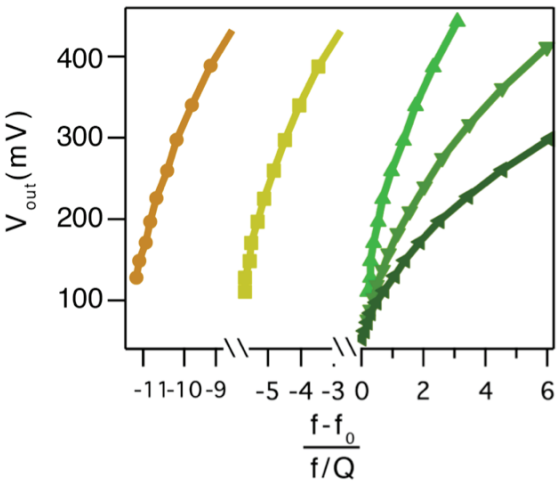


**Figure 5: Nonlinear NEMS oscillator frequency tuning.** "Backbone" (maxima) curves for the nonlinearity parameter, $\alpha$, are shifted by changing oscillator frequency and output voltage.

After preliminary measures were taken to temperature stabilize the oscillator modules, we found that the frequency of an individual oscillator drifts with an average rate of ~1Hz/s. This necessitated repeated retuning of oscillator frequencies. In future implementations, this can be stabilized by more aggressive measures for temperature control and hermetic packaging of the NEMS resonators. The latter is describe in a bit more detail below.

### *NETWORK BOARD*

In our flexible architecture, PCB oscillator modules plug into a network board that provides the network's edges. In present network board embodiments, each oscillator module is coupled solely to its nearest-neighbors. A block diagram of the network board is displayed in Figure 1. The network board is capable of supporting ring network topologies comprising 3, 5, 7, or 8 oscillators. Incoming digital signals from the controller are multiplexed to the network board before being routed to the individual oscillator boards.

### *NETWORK BOARD BENCHMARKING*

Our ring-topology network board permits varying the coupling between oscillators; this coupling constitutes the network's edges. Both the magnitude and phase of this coupling are controllable. Each edge is tested before the oscillator PCBs are inserted into the network board to ensure it is properly configured. However, we found that edge calibration via signal gain *a priori* is inferior to calibration under conditions of operation, using the oscillator dynamics (both individually and in pairs), after the network is fully assembled. This is described in more detail below.

## DIGITAL-TO-ANALOG INTERFACE

The digital-to-analog interface provides connections to digital control components on the oscillator board, and to the digital oscilloscope that provides oscillator module readouts. In Figure 1, the configuration of Raspberry Pi controller within the digital interface is schematically depicted. In operation, this controller does not actually translate digital control signals to implement analog

control of the network; instead it translates the software control commands from the PC into the machine language of the digital step components on the oscillator boards and network PCB.

### *DIGITAL STEP COMPONENTS*

The digital step components give uncertainties, at maximum, of half a step. For the attenuators, this constitutes an uncertainty of ~0.1dB, which yields ~2% uncertainty in nonlinearity $\alpha$ and ~1% in coupling strengths, $\beta$. For the digital potentiometers used in controlling loop phase shift, this corresponds to ~2° uncertainty. For the frequency control, currently this corresponds to 5 Hz uncertainty in shifting the NEMS, which is 1% of $f_0/Q = \delta$. According to the manufacturer's specifications, these values can be altered on a time scale faster than $1\mu s$; this is 1000x faster than the slow-time scale of the oscillator modules, $\tau_s = 1/\delta$.

### *DIGITAL OSCILLOSCOPE*

The analog-to-digital converter we employ is an 8-channel, 20MHz 12-bit USB-3 digital oscilloscope (Picoscope, Inc.; Model PS4284). This oscilloscope can be operated in a single-shot acquisition mode with a maximum time-record depth of 256 million samples. This oscilloscope is capable of streaming data directly to the PC via the USB-3 interface. The digital oscilloscope's interface employs API protocol, accessible via a C programming interface. A Python wrapper is used with the C-language interface.

The oscilloscope can read the NEMS oscillators directly at their fastest nodal frequencies ($f_0 \sim 2MHz$) and stream the sampled output to the PC. We found it possible to execute direct reads in single-shot mode with a rate of one acquisition per 8ms. This latency is due to handshaking between the PC and the oscilloscope; thread latency in the PC is much lower. All data shown in this report is acquired using the single-shot mode.

### *RASPBERRY PI 2 COMMAND TRANSLATOR*

The Raspberry Pi 2 controller is a single-board computer that hosts a Broadcom "system-on-chip" (SoC). The Broadcom SoC can translate commands received via Ethernet (via ssh protocol) into digital words via a GPIO 40-pin header. This 40-pin header includes a serial peripheral interface (SPI) that we employ to control the digital step components on the individual oscillator boards. Custom C-language scripts are used to carry out the translation. For a single ssh command, any digital sequence can run at speeds faster than 5MHz. This is key for executing carefully timed sequences with our networks.

## SOFTWARE/CONTROLLER

To facilitate scalability when moving to larger networks, the controlling software is written using an object-oriented approach using Python 3. Specifically, each component in the network (including the digital controller and readout ADC) is represented by an object in software. Each instantiation of a specific object has intrinsic properties characteristic of that class, and these can be manipulated in real time. There are currently 5 main classes: *rings, nodes, edges, controllers,* and *scopes*. Here the

*ring*s class represents our current overall networks, and it employs objects from the other classes to facilitate the experiment.

To illustrate one example of these classes, the *node* class (which represents our oscillators in software) has properties including: "*current frequency*", "*current amplitude*", "*phase shift setting*", "*attenuator setting*" (which adjusts the current state of nonlinear frequency pulling parameter), and "*frequency-voltage calibration*" (frequency tuning response). All such properties can independently be set for any number of nodes (oscillators) comprising the network. Therefore, upscaling from network topologies with just a few oscillators to those with many oscillators is a simple matter of adjusting loops that create the objects in the ring class.

Each day, before data was acquired, our experiments would commence with auto-calibration via Python scripts to facilitate correcting drifts in the network parameters.

## EXPERIMENTAL ACHIEVEMENTS – RESULTS WITH RING NETWORKS

Here, we discuss experiments on networks of oscillators forming a ring topology. This constitutes a linear chain of oscillators with periodic boundary conditions. In our networks to date, we have solely implemented nearest-neighbor coupling. Ring networks were chosen for validating our network architecture since they permit observation of the rotating wave state, which is one of the most basic steady states beyond that of stationary, fully locked synchronization.[2]

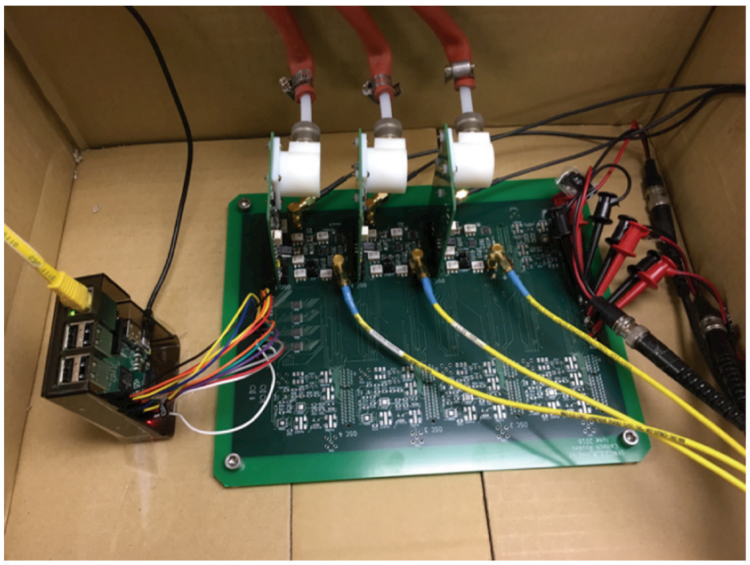

**Figure 6: Experimental setup for a 3-ring network.** On the left side is the Raspberry Pi 2 with its incoming Ethernet connection, and outgoing digital output (multicolored wires). On the far right side are power supply inputs ($\pm 5, \pm 12$). The larger board is designed to hold 3, 5, 7, and 8-ring networks. Bypass resistors interconnect the two furthest oscillator modules. The black cables (upper right) are three SMA coax lines for monitoring NEMS oscillator output, while the three yellow cables are SMA coax lines (bottom right) for inserting signals from external sources. The external inputs are used for system calibration only, but can be used as control input is if desired.

### RESULTS ON A NETWORK OF 3 OSCILLATORS

To gain experience with manipulating and understanding synchronized oscillator networks, we assembled the smallest, 3-oscillator ring network. This implementation allows us to assess the heterogeneity inherent to our experimental design and NEMS device fabrication protocols. Such assessments proved to be of great importance as we worked though the unexpected challenges that arose as we implemented and perfected our new experimental platform.

## *EXPERIMENTAL SETUP*

Hardware for the 3-oscillator network is shown in Figure 6. In this setup, three oscillator boards are configured in a ring topology with a nearest neighbor interactions mediated via a coupling term along each edge. In the equation of motion governing $x_i$, this coupling is proportional to $x_j - x_i$. Note that the coupling term above constitutes purely *reactive* coupling, as it is devoid of velocity components.

Prior to acquiring data, great care was taken to calibrate each node and edge of the 3-ring network. Two major points of importance were discovered in the weeks invested in building our calibration protocols.

First, the susceptibility of each resonator within the oscillator board is only important relative to that of its adjacent neighbors. Since each edge is defined by only a few electronic components and provides no amplification, the variation between edges is smaller than that existing between the nodes. Therefore, we can match all the edges to behave nearly identically (by imposing the same attenuator and phase settings at each edge to realize a specific coupling); subsequently, we adjust components on the nodes to match each other. By following this protocol, calibration proved easier and yielded more homogeneous network nodes and edges.

Second, to achieve optimal results, we find that all of the resonators must be kept *in vacuo* and tuned to the same frequency for several *weeks;* this ensures that their performance stabilizes. Slow drifts in oscillator parameters necessitated repeated adjustment of phase shift for each of the oscillator modules (in addition their back-end calibrations) as they settled. If vacuum was broken, the settling process would begin anew – once operation *in vacuo* was re-initiated, several additional weeks of stabilization would be necessary to converge back to optimal performance. This has led us to pursue our present efforts to “permanently” vacuum-encapsulate the NEMS resonators, incorporating a getter within industry-standard hermetically packaging to provide long-term, high-vacuum environment for their operation. With this in place, along with external temperature stabilization, we believe that the weeks-long process towards parameter stabilization will be circumvented.

## *CALIBRATION*

Precise calibration proves to be extremely important for the 3-ring network; this is in keeping with our previous experience with a coupled pair of oscillators, as explored by Matheny, *et al.* [2]. We find that while significant heterogeneity exists within the network, the synchronization states manifested will not conform to any simple theory.

Our calibration procedure is as follows. First, we adjust VA2 (Figure 3a) until the frequency tuning/voltage-out is the same for each oscillator (light green to dark green, Figure 5). This is one of two parameters that controls the nonlinearity of each node. The other term, the drive output from AGC circuit, is adjusted after calibrating the edges.

After all the oscillators lie along the same curve as in Figure 5, we measure the “self-tuning” along each edge. This means that we measure how much this feedback (*i.e.*, the term in the coupling proportional to $x_i$) tunes the oscillator frequency for both oscillators connected along each of the

network's edges. In essence, when the frequencies of two oscillators are far apart, each edge acts as an additional feedback term that pulls their linear frequencies. We use this to extract the coupling directly, in units of frequency. Our edge calibration procedure has been verified using pair synchronization along the edges in similar fashion as the procedure employed by Matheny, *et al.* [2].

Once all edges have been calibrated, VA4 can be adjusted to bring the oscillators to the same amplitude level. This does not shift the susceptibility of the oscillator relative to the edges/network since it is independent of the coupling loop.

Parameters employed for the 3-ring network range as follows:

- Frequency differences: $\delta \in \{-20, 20\}$
- Nonlinear frequency pulling: $\alpha \in \{0.2, 4\}$
- Reactive coupling strength: $\beta \in \{0.05, 1\}$.

The lower limit of the nonlinear frequency pulling is set by the minimum feedback required to retain 0dB loop gain. Lower values of $\alpha$ can be achieved by increasing gain between the NEMS and the AGC input.

## EXPERIMENTAL RESULTS FOR A 3-RING NETWORK

Theoretically, a 3-ring network with reactive coupling and identical nodal and edge parameters should give rise to three distinct states. The simplest, fully synchronized state occurs when all three phases of the oscillators are fully locked, with zero phase difference between nearest neighbors. The other two states are termed "splay states"; they are *rotating* synchronized states. In these two splay states the oscillator phases rotate around the ring. All three of these states can be observed in real time by evaluating the phase differences between nearest-neighbor nodes. If all nearest-neighbor pairs have the same, stationary, and *non-zero* phase *difference* along each coupling edge in our network, then they are coupled within a stable splay state.

In Figure 7 we show the phase difference $\Delta_{ji}$ for $j = 1, 2, 3$ along the network edges as a function of time, for two experimental runs (Runs 1, 2). In these data traces, the system starts with the following initial conditions: frequency differences less than frequency detuning, $\delta < .01$ ; nonlinearity, $\alpha = 0.2$ ; and coupling $\beta = .05$. At $t = 0.15s$ , we uniformly increase the coupling strength at all edges to $\beta = 0.7$. This induces a transition to a synchronized state. At $t{\sim}0.25s$ , the resonant frequencies are

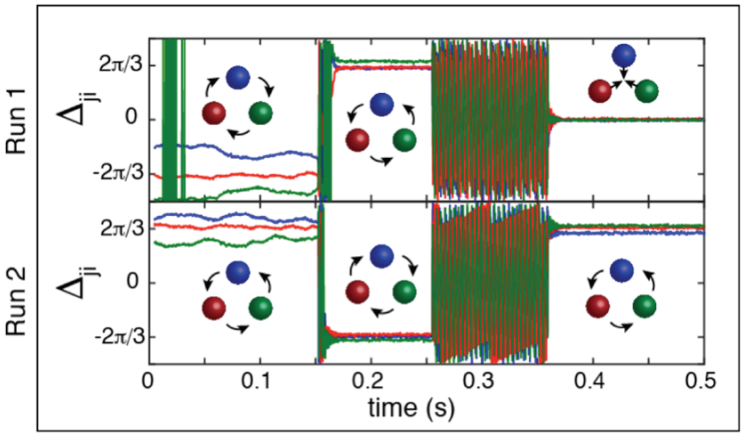


**Figure 7:** Two different experimental runs of the synchronized network showing time-domain dynamics of the phase differences $\Delta_{ji}$ along edges. The system switches between different synchronized states upon shifting of parameters. Here the exact same parameters were used, but the sequence of observed states is different. Note the transients between states.

detuned from each other using the onboard DACs, and this detuned condition is maintained for roughly 0.1s to induce network de-synchronization. Subsequently, at $t{\sim}0.35s$ the resonant frequencies are re-tuned back to their original (common) value. This de-synchronization protocol serves to randomize the network's initial conditions between Runs 1 and 2.

In Figure 7, the red, blue, green balls represent the oscillator nodes within the ring network. In Run 1, the phase differences rotate clockwise. Subsequently, after increasing the strength of edge coupling, the network settles into a state characterized by counter-clockwise rotation of the phase differences. After the initial conditions are randomized, the network re-settles to a different, fully locked state. In the Run 2, with an identical sequence of control parameters as employed for Run 1, the evolution of states is entirely different. Note that the transients between states can be seen and examined to elucidate the evolving dynamics as the network transitions from its uncoupled to synchronized states. This level of detail is unprecedented in experimental studies of synchronization; it has not previously been possible in such an exhaustive manner. This demonstration clearly shows that our network platform provides the complete details of the rich and evolving dynamics within synchronizable systems.

After taking roughly one thousand such runs we can build up a "quasi-potential" picture of the phase space of nearest-neighbor phase differences. These plots elucidate the fascinating trajectories of network-state evolution in the time domain. In Figure 8 we plot the density of all points comprised in this large number of runs. Presenting our data set in this manner illustrates the fact that most points in these trajectories lie near attractors at $0, \pm 2\pi/3$. The tightness (*i.e.*, the localization) of the quasi-potential minima illustrates the homogeneity of our network. Note that assembly of such highly detailed representations of network dynamics would be impossible without acquiring complete time

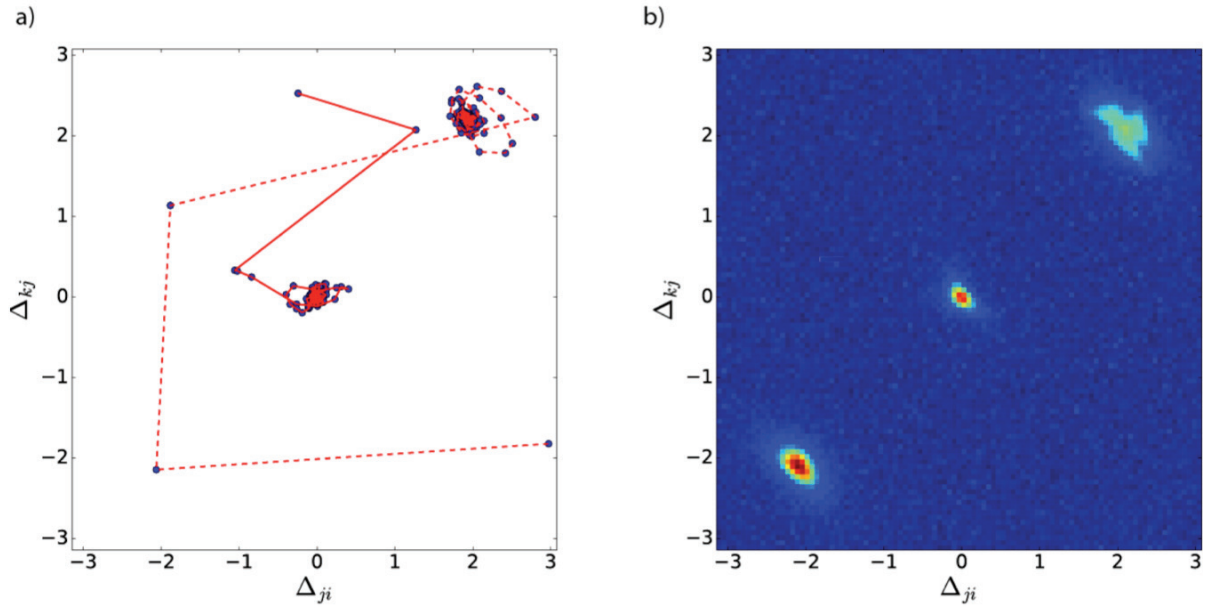


**Figure 8: Time-domain dynamics of 3-oscillator network. a)** Two different experimental runs of the synchronized network showing time-domain dynamics of the phase differences $\Delta_{ji}$ along edges in phase space (red solid, red dashed). The system settles into regions around the stable states. **b)** Density of points along trajectories for 1000 runs. The stable states can be clearly seen.

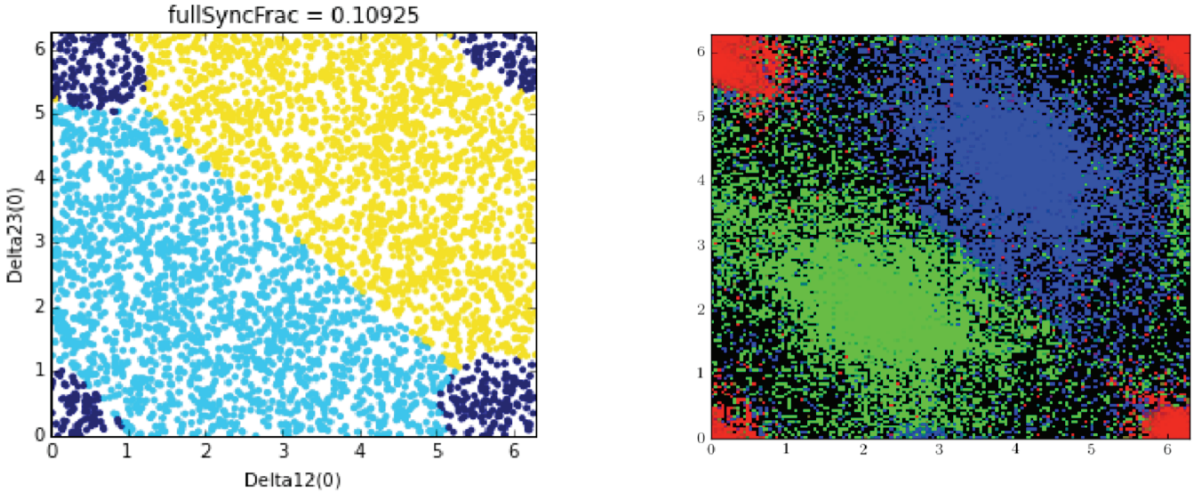


**Figure 9: Basin of attraction for phase differences $\Delta_{12}$ vs $\Delta_{23}$. Left:** The theoretical prediction for the $\alpha = 0.2, \beta = 0.7$ Dark blue are those initial conditions which fall into the fully locked state. Light blue (yellow) are those points which fall into the $\frac{2\pi}{3}(-\frac{2\pi}{3})$. **Right:** Experimental result for the same parameters.

records of all of the network's microscopic edge and node variables, as enabled by our platform.

In Figure 9, we compare the basins of attraction based on the experimental data in Figure 9 with theoretically predicted basins for the same set of parameters. This comparison indicates that noise is not a prevalent factor in these experiments, since the experimentally acquired basins are quite distinct and similar to the (noiseless) theoretical predictions. This comparison of basin plots further demonstrates how closely our experimental 3-ring network matches predictions from theory.

To illustrate the range of parameters accessible to us, we show the phase diagram of synchronized states when nonlinearity ($\alpha$) versus coupling ($\beta$) are swept in the 3-ring network (Figure 10). Green

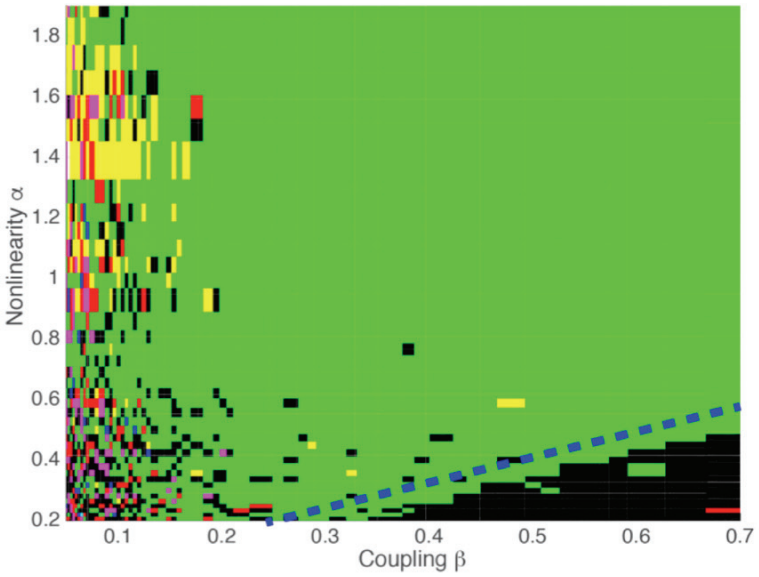


**Figure 10: Synchronization diagram for coupling-nonlinearity phase space.** Green shows parameter values where only the two splay states are found to be stable. Black is parameter values where all three states are found to be stable. The blue dashed line is the theoretical prediction for the boundary of stability for the fully locked state. Note the black region does not meet this prediction since only 10 experimental trials were taken per point in parameter space.

pixels represent situations where only the two splay states can arise, whereas black pixels illustrate parameter values where the two splay states *and* the fully locked state can appear. The blue dashed line (lower right) illustrates the theoretically predicted boundary of stability for the fully locked state. Note that the black region does not quite reach the theoretical limit of stability; but here only 10 experimental trials per point in parameter space were acquired to create a preliminary plot. Therefore, fully locked states within the basin that occur with probability under 10% are unlikely to be evident in this rough diagram. Scattered colors on the left represent parameters for which the system does not lock, presumably due to the system's susceptibility to intrinsic noise in these locales.

## RESULTS WITH A NETWORK OF 8 OSCILLATORS

Having obtained a greater understanding of the challenges to assembling and interrogating nonlinear NEMS ring networks by first working with a 3-ring topology, we constructed an 8-ring network. This was assembled with entirely new components: including NEMS oscillator modules, the network PCB, oscilloscope, and the controller. Without implementing signal multiplexing, this present level of network complexity fully taxes the digital oscilloscope at its capacity (*i.e.*, its acquisition bandwidth). Figure 11 shows the fully populated 8-ring network board. For the data presented, this board had not been under vacuum or DC bias voltages for as long as the 3-ring board (<1 month). Hence, slow drifts in the system had not yet completely settled, but initial data is presented below.

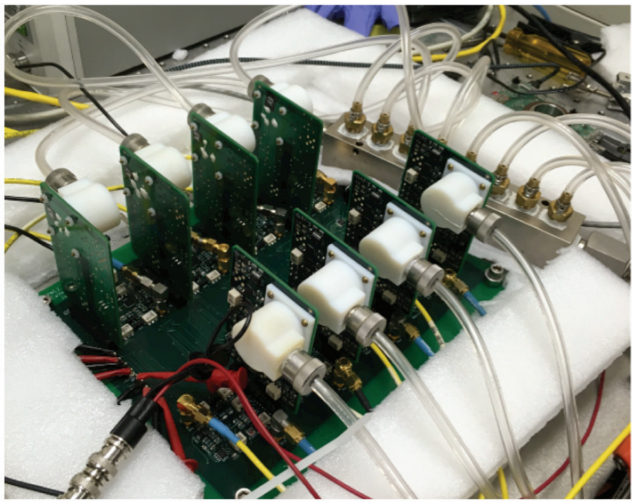

**Figure 11: The 8-oscillator NEMS ring network.** Note the vacuum manifold on the backside of the ring board (top right), which breaks out the vacuum into 8 separate lines terminating at the individual oscillator modules.

We present data for three different trials at fixed values of detuning and nonlinearity: $\beta = 1,\ \alpha = .15$. The data are shown in Figure 12. Here, the only control action implemented occurs at $t \sim 0.2s$ ; at that point in time, the coupling is turned up from $\beta = 0.05$. (The precise time of this imposed transition varies somewhat between trials because, in the present implementation, we had no free channel on which to trigger using the control sequence.) Figure 12 makes it readily evident that the three final states are different splay states. Trial 1 ends in the "anti-ferromagnetic" $\pi$ state, Trial 2 ends in the $\frac{7\pi}{4}$ state, and Trial 3 ends up in the $\frac{3\pi}{4}$ state.

We have chosen the colors in our representation (Figure 12) so that adjacent oscillators pairs in "color space" are spatially proximal (*i.e.,* nearest neighbors) within the network. For example, blue and purple are adjacent oscillators, but blue and yellow are not. This elucidates that nearby oscillators pairs have similar phase differences.

It is evident that the three synchronized final states in these trials show phase differences that are somewhat more disparate than those observed with the 3-ring network (Figure 7). This likely arises

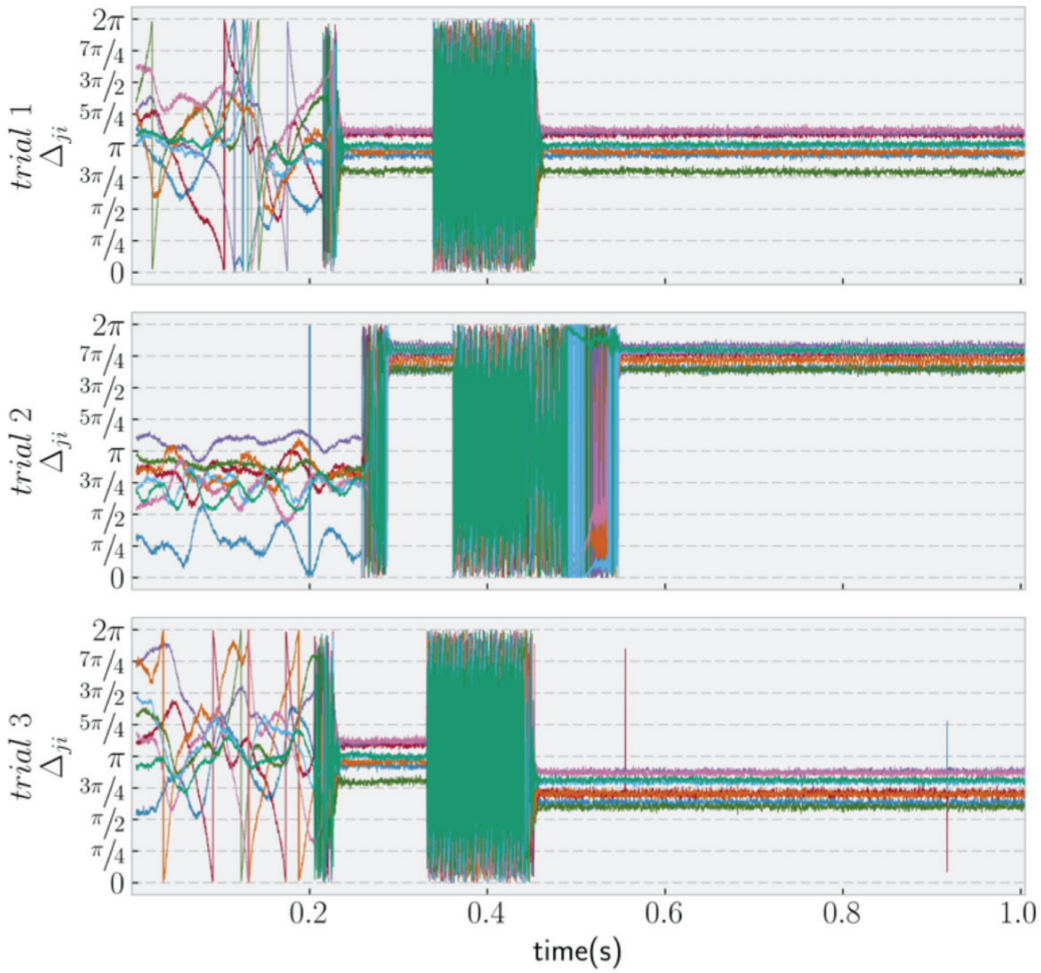


**Figure 12:** Three trial runs of the 8-ring for $\alpha = .15, \beta = 1$. Here the three trials end up in three different splay states. Run 1 ends up in the 'anti-ferromagnetic' $\pi$ state, Run 2 ends up in the $7\pi/4$ state, and Run 3 ends up in the $\frac{3\pi}{4}$ state.

from at least two factors. First, as mentioned above, parameter drifts in this preliminary data acquired from the 8-ring network are *not* likely to have settled sufficiently to permit ideal initial calibration. As mentioned previously, some months may be needed before the devices fully settle ("age") into their ultimate, steady state performance. Second, the synchronized states are indeed less stable for larger rings – and, for these, small network and edge asymmetries likely play an enhanced role. An additional manifestation of this is manifested in the fact that it take a bit longer for the 8-ring network to stabilize into synchronized states than for the case of the 3-ring network.

## CONCLUSION

We have developed a novel and flexible platform for network-based studies of oscillator synchronization that provides full access to all parameters, and permits readout of the time-domain evolution of dynamics – including the fastest dynamics – at each and every node. This platform is completely ready for novel explorations of network phenomena. This entire platform was developed

from the bottom up, using nodes based upon nonlinear NEMS resonators that are incorporated into electrical feedback oscillator circuits. Networks components include: the nonlinear NEMS resonators (frequency selective device), electronic oscillator feedback circuitry, network board multiplexing, digital control electronics, and software designed to enable network control and data acquisition at full bandwidth.

Our piezoelectric NEMS resonators were developed specifically for this program. They have proven ideal for attaining the requirements that we initially delineated as being essential to the success of this effort. These resonators also prove to be robust and, so far, continue to perform ideally even after more than 4 months under constant excitation. Their onset of nonlinearity is at a "comfortably" low driving voltage, relative to the feedback loop and coupling signal levels.

While our initial design for the oscillator and network PCBs were not initially successful, we pursued the implementation of multiple successive generations -- focusing on the incorporation of flexible, digitally steppable components. These ultimately proved capable of providing a large range of parametric tuning. At low inter-oscillator coupling values, synchronization dynamics can be highly compromised by noise. Conversely, at high coupling values, network dynamics in the weak-coupling regime are inaccessible. With our present implementation we can access all ranges in between, to enable exploration of vast regions of interest for real-world networks.

The control electronics developed for the program are based on the Raspberry Pi platform. This permits use of existing C libraries for control of the SoC, to facilitate fast, successive actions of the controller. These routines are immediately translatable to other SoC–based controllers (such as the popular Nvidia Tegra). Also, future integration between the controller and the computer that receives the digital data stream will allow *continuous* feedback control of the network. (In these present demonstrations, only time-stepped changes were implemented.)

Our software, which was developed in Python, is immediately translatable between system architectures without the need for Matlab code. In addition, these routines are upscalable to an arbitrary number of oscillators, as they are implemented with an object-oriented approach in which the network architecture is "copied" into instantiations of "object classes" within the Python environment. This flexibility is directly evidenced in ease of our move from 3 to 8 oscillators without the need for software updating.

Some overarching insights into experimentally realized, synchronized oscillator networks can be extracted from our effort:

1) It was learned throughout the course of the program that while resonators coupled laterally on-chip might be able to be matched in frequency; other parameters (especially $S_{21}$ and nonlinearity) are extremely hard to control with this type of resonator due to device-to-device stress variations (Figure 2) across the wafer. With the level of mismatch currently inherent with our resonators, it would not have been possible to just "turn them on" and then understand the dynamics emerging from networks with many oscillators. (Note that in our 8-node network (Figure 8) we have achieved a very close set of initial parameters). Efforts to reduce fabrication-induced resonator variations to suppress network inhomogeneities will be important in future work.

2) When the "external" tuning approach is taken to reducing the inhomogeneities that are initially present in network constituents, drifts in nodal frequencies, which occur on the time scale of minutes, must be corrected for continuously. Additionally, long-term drifts in other resonator parameters can occur over intervals spanning from weeks to months; these must be ameliorated before constant tuning is implemented.

3) Calibration for synchronization parameters should occur after the whole circuit is assembled and turned on. For example, discrepancies between the loop gain found from a driven response in the coupling branch back into the oscillator does not provide as good a calibration as using the coupling to tune the oscillator.

4) Digital step components are much more robust and reliable than the continuously variable attenuators and phase shifters we initially employed in the early phases of this effort.

5) NEMs oscillators operating from 1-10 MHz with *Q*'s of 1,000–10,000 provide a convenient time scale (for fast dynamics, for energy damping, and for slow-time network phenomena) to observe dynamics relative to the other ADC/DAC hardware available.

6) Synchronization transients can be useful for mapping out state dynamics (Figure 8).

7) Theoretical models based on homogeneous networks can match acquired experimental data quite closely (Figures 9, 10).

8) Noise evidently becomes more important as the size of the network grows (Figure 12). The effective phase space in small rings can be explored with this approach since the parameter space becomes "squeezed" by the noise (Figure 10, 12).

## REFERENCES

1. Matthew H. Matheny, Warren Fon, Michael C. Cross, and Michael L. Roukes, *ARO Progress Report, Contract No. W911NF1310240, 4 November 2015*.

2. Matthew H. Matheny, Matt Grau, Luis G. Villanueva, Rassul B. Karabalin M.C. Cross, and Michael L. Roukes, *Phase Synchronization of Two Anharmonic Nanomechanical Oscillators*. Physical Review Letters 112, 014101 (2014).

3. Jeffrey Emenheiser, Airlie Chapman, Márton Pósfai, James P. Crutchfield, Mehran Mesbahi, and Raissa M. D'Souza. *Patterns of patterns of synchronization: Noise induced attractor switching in rings of coupled nonlinear oscillators.* Chaos: An Interdisciplinary Journal of Nonlinear Science **26**, no. 9 (2016): 094816.

4. Warren Fon, Matthew H. Matheny, Jarvis Li, Lev Krayzman, Michael C. Cross, Raissa M. D'Souza, James P. Crutchfield, and Michael L. Roukes, *Complex dynamical networks constructed with fully controllable nonlinear nanomechanical oscillators*, submitted to Nano Letters (2017).